www.czasopisma.pan.pl PAN POLSKA AKADEMIA NAUK www.journals.pan.pl

A R C H I V E S O F M E T A L L U R G Y A N D M A T E R I A L S

Volume 60 2015 Issue 4

DOI: 10.1515/amm-2015-0457

J. BARGLIK*, A. SMALCERZ*#, A. SMAGÓR*, P. PASZEK*

ANALYSIS OF CONTINUOUS INDUCTION HARDENING OF STEEL CYLINDER ELEMENT MADE OF STEEL 38Mn6

ANALIZA PRZELOTOWEGO HARTOWANIA INDUKCYJNEGO WALCA ZE STALI 38Mn6

The paper presents analysis of surface induction hardening of a cylindrical element made of steel 38Mn6. The mathematical model of the non-stationary process is elaborated. Calculations of coupled electromagnetic and temperature fields are provided by means of the Flux 2D software. Computations are compared with the measurements realized at the laboratory stand located in the Silesian University of Technology. The expected hardness distribution within the surface layer is noticed.

Keywords: induction hardening, temperature field, simulation, electromagnetic field

W artykule przedstawiono analizę indukcyjnego hartowania powierzchniowego elementu cylindrycznego wykonanego ze stali 38Mn6. Do obliczeń opracowano model matematyczny niestacjonarnego procesu hartowania. Obliczenia sprzężonych pól elektromagnetycznych i temperatury wykonano za pomocą oprogramowania Flux 2D. Obliczenia zostały porównane z pomiarami na stanowisku laboratoryjnym, które znajduje się w Politechnice Śląskiej. Celem badań było uzyskanie odpowiedniego rozkładu twardości w warstwie powierzchniowej.

1. Introduction

Induction surface hardening is a kind of the heat treatment technology where only a working surface layer of the steel element or its selected part is heated inductively and then immediately cooled by merging into a quenchant or by spraying while remaining parts of the element are practically not treated. As a result a thin surface layer with required values of hardness and microstructure is obtained [1-5]. The internal part of the treated element remains soft with not changed values of hardness and with the practically the same microstructure as before starting the process. The carburization is typically used as the conventional surface hardening method. It is characterized by a treatment of the element at a high temperature for several hours in a carbonaceous atmosphere. This method is characterized by high quality, but its important disadvantage is a huge energy consumption. Similar features of the quality of the treated element, but with a several times lower specific energy consumption could be achieved by means of induction surface hardening [6-10].

The induction surface hardening process consists of two consecutive stages with a short technological break between them. First the hardened element is heated inductively during as short as possible period of time (often not more than a second or a couple of seconds) to the hardening temperature. Then after a short break necessary for switching off the inductor and its removal the element is immediately cooled by a suitable quenchant. Due to big heating rates characteristic for induction heating in order to obtain the uniform austenite microstructure before quenching it is necessary to heat the element to the temperature distinctly bigger than the classical austenization temperature Ac3. The austenization temperature for induction surface hardening depends on speed of heating and in order to avoid taking to computations incorrect data the best solution is to determine it by measurements. More detailed description of physical background of the induction surface hardening process as well as some practical examples are presented for instance in [11-15]. An obstacle in application of modern induction surface hardening technologies to industry seems to be a lack of precise and simple computation methods facilitating design, control and exploitation of such devices. From the other side the development of information technology creates better and better conditions for mathematical modelling of various, even complicated technological processes. For engineering computations the most suitable seem to be FEM based numerical methods making possible to calculate selected parameters of the process with the expected accuracy. However the modelling of the induction surface hardening is still a challenge and requires many new research activities [16-20].

* SILESIAN UNIVERSITY OF TECHNOLOGY, FACULTY OF MATERIAL SCIENCE AND METALLURGY, DEPARTMENT OF COMPUTER SCIENCE, 8 KRASIŃSKIEGO, 40-019 KATOWICE STR.POLAND

Corresponding author:albert.smalcerz@polsl.pl

The paper presents numerical modelling of induction surface hardening process of steel cylinder. The computations are compared with experiments provided at a laboratory stand. First a short description of the technical problem is provided, then the mathematical model is described, next some computations are presented and compared with the measurements. And finally the conclusions and aims of further research activities are formulated.

2. Description of the technical problem

The technical problem presented in the paper is to propose the induction surface hardening system for the steel cylinder being a part of the classical Rack & Pinion gear used in automotive industry (Fig.1 left). The geometry hardened layer is depicted in Fig. 1 right.

Fig. 1. View of steel cylinder used for investigations (left) and its geometry (right)

The geometry of the investigation element is shown in Fig. 2. Basic dimensions of the element are as follows:

- total length of the element $l = 85$ mm,
- length of its cylindrical part $lc = 52$ mm,
- length of hardened layer $lh = 40$ mm,
- thickness of hardening layer $b = 0.6$ mm,
- diameter of toothed part $D = 12$ mm,
- diameter of cylindrical part 8 mm.

The material properties and their dependence on temperature is collected in Tab.1.

The element is made of steel 38Mn6. The hardening layer is required to be complete hardening with the martensite microstructure and the hardness of 52 - 56 Rockwell degrees (HRC). The chemical composition of the investigated steel is as follows: 0.34 – 0.42 % C, ≤0.4 % Cr, ≤0.1 % Mo, 1.40 – 1.65 % Mn, 0.15 - 0.35 % Si, ≤0.035 % P, ≤0.035 % S, and ≤0.63 % Ni.

The relative magnetic permeability is assumed as equal to $\mu r = 100$. The austenitizing temperature of the steel is approximately 820÷850 °C. For fast induction heating (heating rate $vh = 200$°C/s) it is necessary to take bigger value of the modified austenization temperature. Finally the hardening temperature $Th = 910$°C. The process is realized as continual. The view of inductor-sprayer system and its principal dimensions are shown in Fig.3.

Fig. 3. View of inductor-sprayer system

Basic dimensions of inductor-sprayer system as follows:

- total length of the element $l = 150$ mm,
- distance between busbars $Db = 4$ mm,
- height of inductor $h = 10$ mm,
- width of inductor $b = 5$ mm,
- diameter of inductor part 20 mm,
- diameter of sprayer part 37 mm.

The induction heating is provided by one coil ring inductor. Cooling is realized by spraying. As a quenchant the polymer solution Osmanil E2 is applied.

3. Mathematical and numerical models

The mathematical model of the continuous induction surface hardening is given by a set of non-linear and non-stationary partial differential equations for electromagnetic and temperature fields. Both fields may be considered as direct coupled [21-30].

The electromagnetic field is described by the equation for the magnetic vector potential $\boldsymbol{A}$

TABLE 1

Material properties of steel 38Mn6

Temperature,°C	Coef. of thermal expansion, $10^{-6}\times K^{-1}$	Thermal conduction, $W\cdot m^{-1}\cdot K^{-1}$	Specific heat, $J\cdot kg^{-1}\cdot K^{-1}$	Electrical conductivity, $MS\cdot m^{-1}$	Density, $kg\cdot m^{-3}$
20	11.9	46.7	461	4.48	7820
100	12.5	47.8	496	3.73	-
200	13	46.7	533	2.96	-
300	13.6	44.1	568	2.35	-
400	14.1	41.1	611	1.89	-
500	14.5	38.2	677	1.55	-
600	14.9	35.3	778	1.27	-
700	15.4	32.4	884	1.04	-

$$\operatorname{curl}\left(\frac{1}{\mu}\operatorname{curl} \boldsymbol{A}\right)+\gamma\left(\frac{\partial \boldsymbol{A}}{\partial t}+\boldsymbol{v}\times\operatorname{curl} \boldsymbol{A}\right)=\boldsymbol{J}_{\mathrm{z}} \tag{1}$$

where γ denotes the electrical conductivity, μ is the magnetic permeability, $\boldsymbol{v}$ – velocity of inductor sprayer movement and $\boldsymbol{J}_{\mathrm{z}}$ field current density in the inductor.

The solution of (1) is still very complicated and time consuming. The reason of that is too big disproportion between the field current frequency f being in a range of hundreds kHz (it means a period of ms or less) and time of heating equal to several seconds (often even less). Such a problem formulation requires a big number of the time steps and taking into account non-linear dependence of the magnetic permeability on the induction flux density. There is a reason to introduce the next simplification: to consider the electromagnetic field as harmonic and describe it by the Helmholtz equation for the phasor of the magnetic vector potential $\underline{\boldsymbol{A}}$

$$\operatorname{curl}\left(\operatorname{curl}\underline{\boldsymbol{A}}\right)+\mathrm{j}\cdot(\omega\gamma\mu\underline{\boldsymbol{A}}+v\times\operatorname{curl}\underline{\boldsymbol{A}})=\mu\underline{\boldsymbol{J}}_{\mathrm{z}} \tag{2}$$

where j denotes the imaginary unit and ω is the angular frequency.

However it means that the magnetic permeability may be considered as constant in any cell of the discretization mesh. Eddy current density induced in the element is given by (3)

$$\underline{\boldsymbol{J}}_{\mathrm{ind}}=\mathrm{j}\cdot\omega\gamma\underline{\boldsymbol{A}} \tag{3}$$

At the external artificial boundary taken at a sufficient distance from the inductor-sprayer system the Dirichlet condition for the phasor of the magnetic vector potential $\underline{\boldsymbol{A}}=\underline{\boldsymbol{0}}$ is applied. The analyzed problem is axi-symmetric. So the magnetic vector potential has only one nonzero component and equation (2) may be considered as the scalar equation for the tangential component of the magnetic vector potential.

Distribution of non-stationary temperature field in the element is given by the Fourier-Kirchhoff equation:

$$\operatorname{div}\left(\lambda\operatorname{grad}T\right)-\rho c_{p}\frac{\partial T}{\partial t}=-p_{\mathrm{v}} \tag{4}$$

where λ denotes heat conduction, ρ is the density, c_p is the specific heat at constant pressure and p_{v} is the volumetric power density generated by the electromagnetic field.

The volumetric power density consists of the parts: the Joule losses and the hysteresis losses. The volumetric Joule losses w_{J} are given by (5)

$$p_{\mathrm{J}}=\frac{\left|\underline{\boldsymbol{J}}_{\mathrm{ind}}\right|^{2}}{\gamma} \tag{5}$$

The volumetric hysteresis losses p_{H} may be determined by measurements. For the analyzed problem they can be neglected as very low in the comparison with the volumetric Joule losses. The boundary condition along the surface of the element is given by the convection and radiation [30].

$$-\lambda\frac{\partial T}{\partial n}=\alpha_{\mathrm{c,h}}\left(T-T_{\mathrm{c}}\right)+\sigma_{\mathrm{o}}\cdot\varepsilon\cdot\left(T^{4}-T_{\mathrm{r}}^{4}\right) \tag{6}$$

where n denotes the unit outward normal, $\alpha_{\mathrm{c,h}}$ is the convection heat transfer, T_{c} is the temperature of the convection surroundings, σ_{o} is the Stefan-Boltzmann constant, ε is the total emissivity of radiation surfaces, T_{r} represents the temperature of the surrounding radiation surface.

In case of the discussed problem as the radiation surface the internal surface of the coil is taken. For cooling the equation (4) is modified by neglecting the right hand term pv. The boundary condition along the surface of the element is given by convection only.

$$-\lambda\frac{\partial T}{\partial n}=\alpha_{\mathrm{c,c}}\left(T-T_{\mathrm{q}}\right) \tag{7}$$

where $\alpha_{\mathrm{c,c}}$ denotes the convention heat transfer coefficient for intensive cooling, T_{q} temperature of quenchant.

All material properties and heat transfer parameters are considered as temperature-dependent.

The numerical model is shown in Fig. 4.

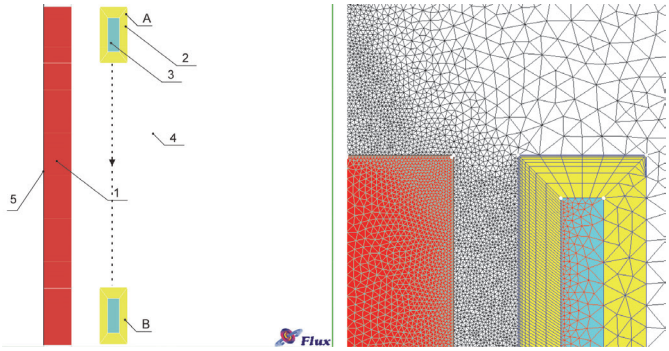

Fig. 4. The calculation model (on left) and meshing (on right) 1 – element, 2 – coil, 3 – sprayer, 4 – air, 5 – axis of symmetry, A, B initial and final position of inductor respectively

For each subdomain the non stationary induction heating is provided and then its stationary cooling. As the initial temperature of the next step the final distribution of the previous step is taken.

4. Computations and measurements

Several simulations are provided by means of 2D Flux software. Computations are verified by measurements realized at the laboratory stand located in the Silesian University of Technology. In order to evaluate the induction surface hardening process some points for a comparison of calculated and measured temperature are selected (their location is shown in Fig. 5). Calculation points are located in two groups:

- at the surface of cylinder in the middle of each part (S1 ,S4),
- at the surface of the cylinder but at one part only (P1 ,P4).

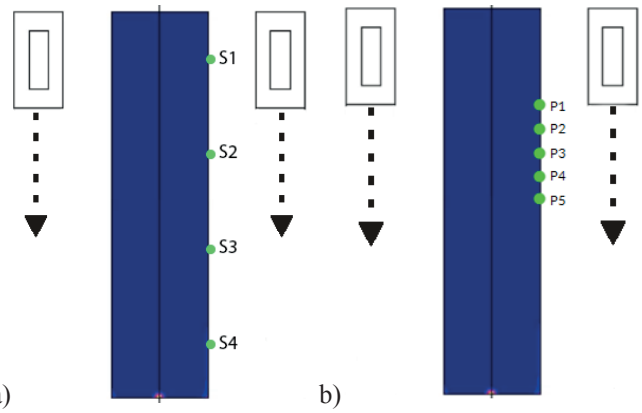

Fig. 5. Location of points selected for comparison of calculated and measured temperature a) S1 - S4 b) P1 - P5

Measurements are provided at the universal laboratory stand equipped with transistor generator MOSFET of 10 kW power and nominal frequency 300 – 500 kHz. The device makes possible to control a precise location of inductor with respect to the element, regulation of movement and if necessary also rotation velocity. Some parameters are presented in Tab.2

TABLE 2

Cases of calculations

Power, kW	Flow-rate, l/ min	Velocity, mm/s	Current, A	Frequency, kHz
9	6.4	5	910	454

A way of computations is presented in Fig. 6.

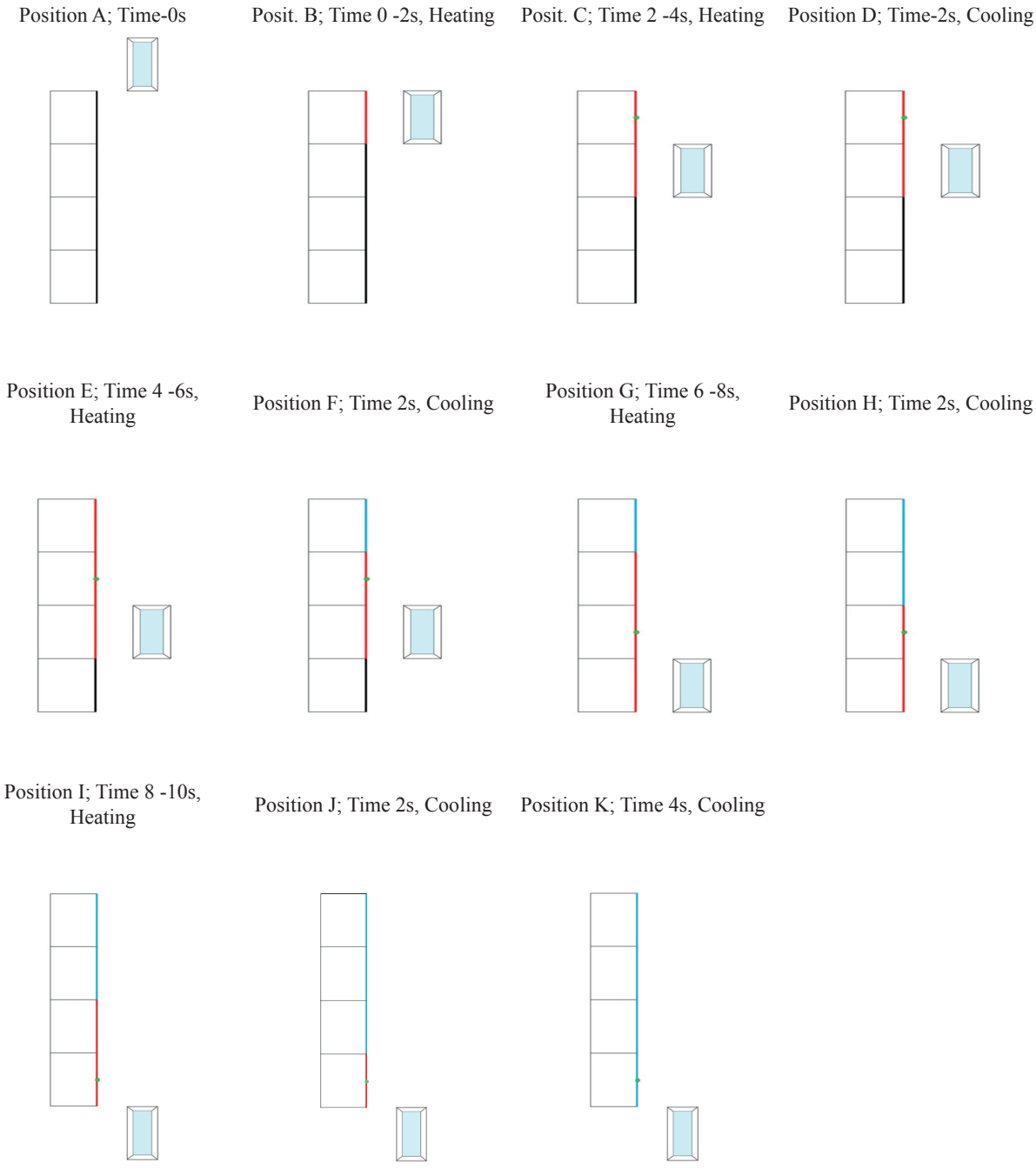

Fig. 6. A way of calculation – position of inductor red colour means heating, blue colour cooling

Results of temperature computations are presented in Figs. 7 – 8. Total time being a sum of non-stationary heating and stationary cooling is equal to 22 s. Temperature dependence on time for four points S1 – S4 is presented in Fig. 7. Analyzed positions A – K representing continual heating and stationary cooling are depicted and explained in Fig.6.

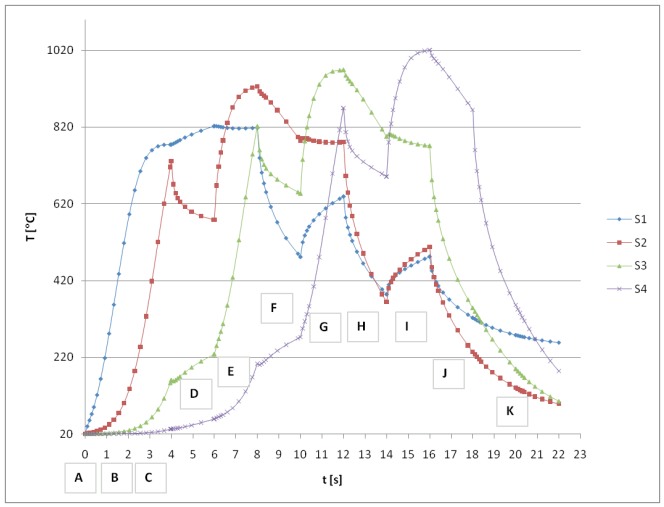

Fig. 7. Temperature dependence on time for four points S1 - S4

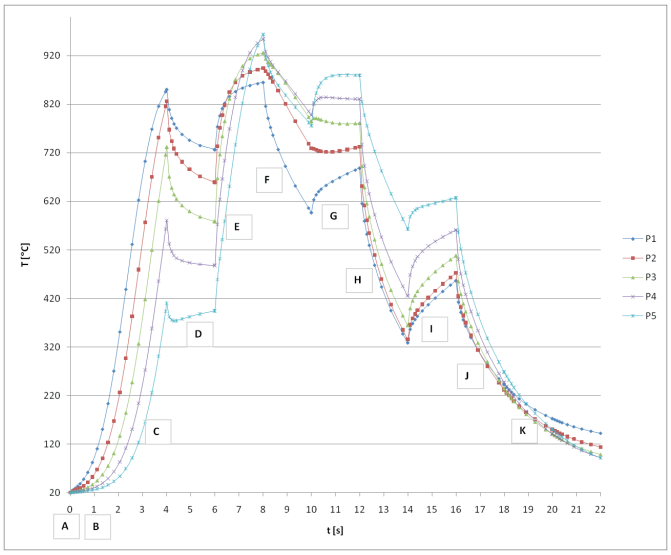

Fig. 8. Temperature dependence on time for five points P1 - P5

Computations are compared with measurements. Results of temperature measurements are presented in Fig. 9. Quite reasonable agreement between calculations and measurements is noticed (Fig. 10) however is necessary to mention that the accuracy of temperature measurement is not recognized exactly. And finally the hardness distribution are measured (Fig. 11). The expected hardness distribution in the cross section of the element is obtained. The hardness on the surface is equal to 53 Rockwell degrees (HRC) and thinness of the hardened layer is equal to 0.6 mm.

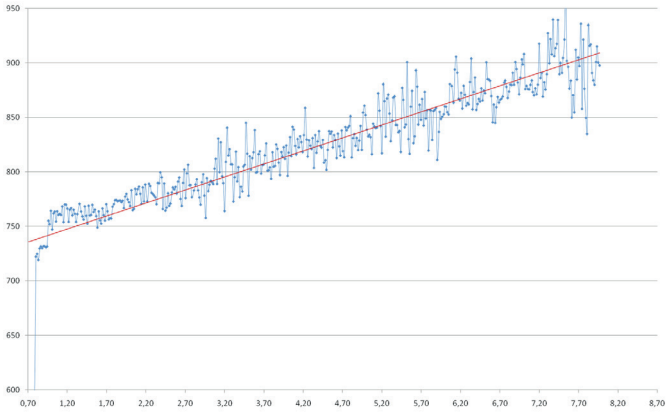

Fig. 9. Time dependence of temperature measured by pyrometer

Comparison of computations and measurements is presented in Fig.10 .

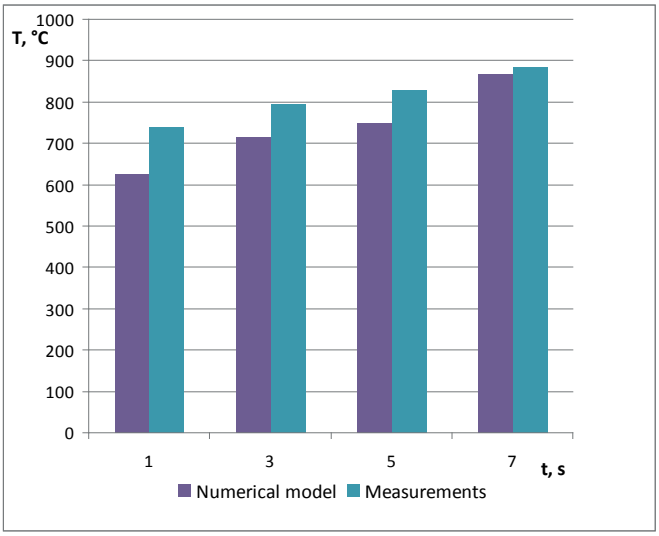

Fig. 10. Comparison between computations and measurements

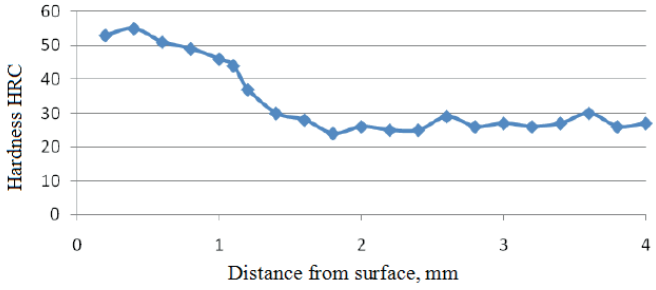

Fig. 11. Hardness distribution within a cross section of the element

5. Conclusions

The paper presents analysis of surface induction hardening of a cylindrical element made of steel 38Mn6. The mathematical model of the non-stationary process is elaborated. Calculations of coupled electromagnetic and temperature fields are provided by means of the Flux 2D software. In order to simplify the computations modeling of induction heating is realized as continual however cooling is

analyzed as stationary. In fact it means division of total time of heating and cooling for eleven two seconds time steps. In order to increase the accuracy the number of time steps should be increased. Computations are compared with the measurements realized at the laboratory stand located in the Silesian University of Technology. Reasonable accordance between computations and measurements. The expected hardness distribution microstructure and thickness of hardened layer is obtained.

Acknowledgements

The study was conducted under the Research Project No. PBS2/A5/41/2014, financed by the National Research and Development Centre – Poland.

REFERENCES

[1] V. Rudnev, D. Loveless, R. Cook, M. Black, Heat Treatment of Metals 4, 97-103 (2003).
[2] D. Rodman, C. Krause, F. Nurnberger, FW. Bach, K. Haskamp, M. Kastner, E. Reithmeier, Steel. Res. Int. **82**, 329-336 (2011).
[3] J. Grum, V. Rudnev, Int. J. Mater. Prod. Tec. **29**, 1-8 (2007).
[4] D. Rodman, B. Boiarkin, F. Nurnberger, A. Dalinger, M. Schaper, Steel Res Int **85**, 741-755 (2014).
[5] D. Rodman, F. Nurnberger, A. Dalinger, M. Schaper, C. Krause, M. Kastner, E. Reithmeier, Steel. Res. Int. **85**, 415-425 (2014).
[6] B. Oleksiak, A. Blacha-Grzechnik, G. Siwiec, Metalurgija **51**, 298-300 (2012).
[7] J. Labaj, B. Oleksiak, G. Siwiec, *Metalurgija* **50**, 173-175 (2011).
[8] T. Maciag, A. Debski, K. Rzyman, Arch. Metal. Mater. **56**, 585-592 (2013).
[9] M. Saternus, T. Merder, P. Warzecha, Sol. St. Phen. **176**, 1-10 (2011).
[10] A. Glowacz, A. Głowacz, P Korohoda, Arch. Metal. Mater. **59**, 31-34 (2014).
[11] V. Savaria, H. Monajati, F. Bridier, P. Bocher, J. Mater. Process. Tech. **220**, 113-123 (2015).
[12] A. Kohli, H. Singh, Sadhana-Acad P. Eng. S. **36**, 141-152 (2011).
[13] MH. Kim, KY. Rhee, YN. Paik, JS. Hong, YS. Ham, J. Mat. Sci. Eng. A-struct **485**, 31-38 (2008).
[14] J. Grum, Int. J. Mater. Prod. Tec. **29**, 9-42 (2007).
[15] M. Schwenk, J. Hoffmeister, V. Schulze, J. Mater. Eng. Perform. **22**, 1861-1870 (2013).
[16] H. Kristoffersen, P. Vomacka, Mater Design **22**, 637-644 (2001).
[17] D. Homberg, Siam J Control Optim **42**, 1087-1117 (2003).
[18] J. Grum, Int J Mater Prod Tec **29**, 200-210 (2007).
[19] R. Autay, R. Kchaou F. Dammak, P. I. Mech. Eng. J-J Eng. **229**, 115-125 (2015).
[20] M. Niklewicz, A. Smalcerz, A. Kurek, Prz Elektrotechniczny **84**, 219-224 (2008).
[21] D. Coupard, T. Palin-luc, P. Bristiel,V. Ji, C. Dumas, Mat. Sci. Eng. A-struct. **487**, 328-339 (2008).
[22] A. Fornalczyk, S. Golak, M. Saternus, Math. Probl. Eng. ID 461085 (2013).
[23] A. Smalcerz R. Przylucki, Int. J. Thermophys. **34**, 667-679 (2013).
[24] D. Hoemberg, T. Petzold, E. Rocca, Nonlinear Anal-Real. **22**, 84-97 (2015).
[25] J. Barglik, M. Czerwinski, M. Hering, M. Wesolowski, Chapter in IOS Press **29**, 202-211 (2008).
[26] A. Candeo, C. Ducassy, P. Bocher, F. Dughiero, IEEE T. Magn. **47**, 918-921 (2011).
[27] S. Golak, R. Przylucki, J. Barglik, Arch. Metall. Mater. **59**, 287-292 (2014).
[28] K. Gao, XP. Qin, Z. Wang, H. Chen, SX Zhu, YX Liu, YL Song, J. Mater. Process. Tech. **214**, 2425-2433 (2014).
[29] J. Barglik, A. Smalcerz R. Przylucki, J.Comput. Appl. Math. **270**, 231-240 (2014).
[30] A. Smalcerz, R. Przylucki, Metalurgija **52**, 223-226 (2013).

Received: 20 October 2015.